Journal of Ceramic Processing Research. Vol. 16, No. 3, pp. 346~351 (2015)

J O U R N A L O F
Ceramic Processing Research

Properties of nanostructured TiC and TiC-FeAl hard materials rapidly sintered by the high frequency induction heating

Bong-Won Kwak[a], Byung-Su Kim[b] and In-Jin Shon[a,*]

[a]*Division of Advanced Materials Engineering and the Research Center of Advanced Materials Development, Engineering College, Chonbuk National University, Chonbuk 561-756, Korea*

[b]*Minerals Resources Research Division, Korea Institute of Geoscience and Mineral Resources , Daejeon, 305-350, Korea*

In the case of cemented TiC, Ni or Co is added as a binder for the formation of composite structures. However, the high cost of Ni or Co and the low corrosion resistance of the TiC-Ni and TiC-Co cermets have generated interest in recent years for alternative binder phases. In this study, FeAl was used as a novel binder and consolidated by the high frequency induction heated sintering (HFIHS) method. Highly dense TiC-FeAl with a relative density of up to 100% was obtained within 2 min by HFIHS under a pressure of 80 MPa. The method was found to enable not only the rapid densification but also the inhibition of grain growth preserving the nano-scale microstructure. The addition of FeAl to TiC enhanced the toughness without great decrease of hardness due to crack deflection and increase of relative density.

Key words: Nanomaterials, Sintering, Hardness, Fracture toughness, Hard materials.

Introduction

The attractive properties of titanium carbide are high hardness, low density, relatively high thermal and electrical conductivities. TiC is also very stable, with a melting temperature of 2727 K, and does not undergo phase transformations. These properties have seen it used extensively in cutting tool and abrasive materials in composite with a binder metal, such as Ni or Co. The binder phase has inferior chemical characteristics compared to the carbide phase. Most notably, corrosion and oxidation occur preferentially in the binder phase [1]. Hence, the high cost of Ni or Co and the low corrosion resistance of the TiC-Ni or TiC-Co cermet have generated interest in recent years to find alternative binder phases [2, 3]. It has been reported that aluminides show a higher oxidation resistance, a higher hardness and a cheaper materials compared to Ni or Co [4].

The improvement of mechanical properties and stability of cemented carbides could be achieved through microstructural changes such as grain size refinement [5, 6]. Nanocrystalline materials have received much attention as advanced engineering materials with improved physical and mechanical properties [7, 8]. Since they possess a high strength and hardness as well as excellent ductility and toughness, they have garnered more attention recently [9, 10]. Recently, nanocrystalline powders have been produced by high-energy milling [11, 12]. The sintering temperature of high-energy mechanically milled powder is lower than that of unmilled powder due to the increased reactivity, internal and surface energies, and surface area of the milled powder, which contribute to its so-called mechanical activation [13-15]. However, the use of conventional methods to consolidate nanopowders often leads to grain growth due to the extended time for sintering. Generally, the grain growth could be minimized by sintering at lower temperatures and for shorter times. In this regard, the high frequency induction heated sintering (HFIHS) technique has been shown to be effective in the sintering of nanostructured materials in a very short time (typically within 1 minute) [16-19].

We present here the results of the sintering of TiC and TiC-FeAl composites by a high frequency induction heated sintering with simultaneous application of induced current and high-pressure. The goal of this study was to produce dense and nanocrystalline TiC and TiC-FeAl hard materials in very short sintering times (< 2 min). The effect of novel FeAl binder on the mechanical properties, sintering behavior and relative density of TiC-FeAl composites was also examined.

Experimental Procedures

The TiC powder used in this research was supplied by Treibacher Industry AG (Germany). The average particle size was about 1.4 μm and the purity was 99%. FeAl (<45 μm, 99% pure, Sejong Co.) was used as binder material. Powders of three compositions corresponding to TiC, TiC-5 vol.% FeAl, and TiC-10 vol.% FeAl were prepared by weighing and milled in a high-energy ball

*Corresponding author:
Tel : +82-63-270-2381
Fax: +82-63-270-2386
E-mail: ijshon@chonbuk.ac.kr

mill (Pulverisette-5 planetary mill) at 250 rpm for 10 h. WC balls (9 mm in diameter) were used in a sealed cylindrical stainless steel vial under an argon atmosphere. The weight ratio of balls-to-powder was 30 : 1. The grain size of the powders was calculated from the full width at half-maximum (FWHM) of the diffraction peak by Suryanarayana and Grant Norton's formula [20].

$$B_r\,(B_{crystalline}+B_{strain})\cos\theta = k\,\lambda / L + \eta\sin\theta \qquad (1)$$

where B_r is the full width at half-maximum (FWHM) of the diffraction peak after instrumental correction; $B_{crystalline}$ and B_{strain} are FWHM caused by small grain size and internal stress, respectively; k is constant (with a value of 0.9); λ is wavelength of the X-ray radiation; L and η are grain size and internal strain, respectively; and θ is the Bragg angle. The parameters B and B_r follow Cauchy's form with the relationship: $B = B_r + B_s$, where B and B_s are the FWHM of the broadened Bragg peaks and the standard sample's Bragg peaks, respectively.

The milled powders were placed in a graphite die (outside diameter, 35 mm; inside diameter, 10 mm; height, 40 mm) and then introduced into the high frequency induction heated sintering (HFIHS) system made by Eltek Co. in the Republic of Korea. A schematic diagram of this system is shown in Fig. 1. The HFIHS apparatus includes a 15 kW power supply and a uniaxial press with a maximum load of 50 kN. The system was first evacuated and a uniaxial pressure of 80 MPa was applied. A induced current was then activated and maintained until the densification rate became negligible, as indicated by the observed shrinkage of the sample. Sample shrinkage was measured in real time by a linear gauge measuring the vertical displacement. Temperature was measured by a pyrometer focused on the surface of the graphite die. A temperature gradient from the surface to the center of the sample is dependent on the heating rate, the electrical and thermal conductivities of the compact, and its relative density. The heating rates were approximately 1100 ^{o}K minute^{-1} during the process. At the end of the process, the current was turned off and the sample was allowed to cool to room temperature. The entire process of densification using the HFIHS technique consists of four major control stages: chamber evacuation, pressure application, power application, and cooling off. The process was carried out under a vacuum of 5.33 Pa.

The relative densities of the sintered samples were measured by the Archimedes method. Microstructural information was obtained from the product samples, which had been polished and etched, using Murakami's reagent (10 g potassium ferricyanide, 10 g sodium hydroxide, and 100 ml water), for 1-2 minutes at room temperature. Compositional and microstructural analyses of the samples were carried out through X-ray diffraction (XRD), and field-emission scanning electron microscopy (FE-SEM). Vickers hardness was measured by performing indentations at a load of 30 kg_f with a dwell time of 15 s.

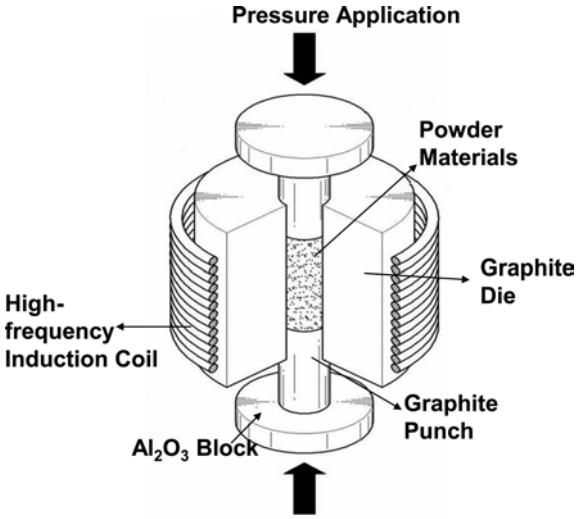

Fig. 1. Schematic diagram of apparatus for high frequency induction heated sintering.

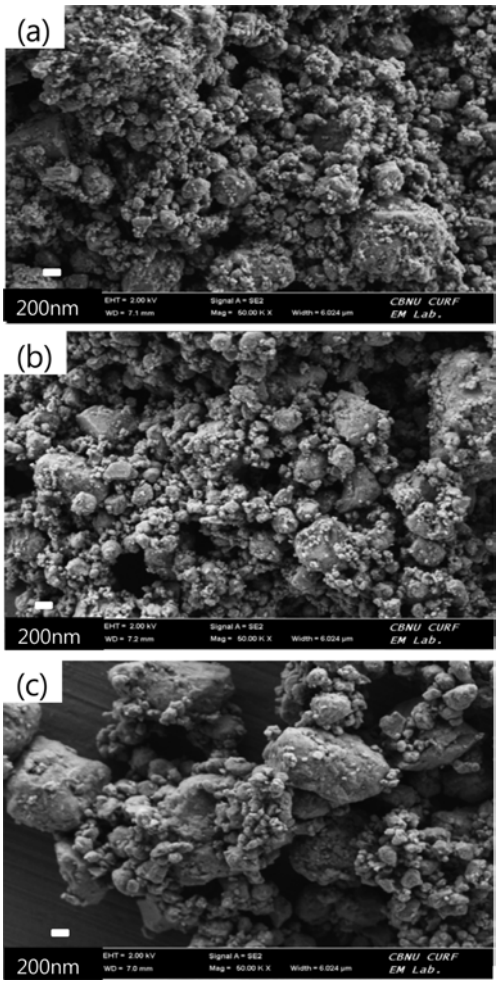

Fig. 2. FE-SEM images of powders milled for 10 h; (a) TiC, (b) TiC-5 vol.%FeAl, and (c) TiC-10 vol.%FeAl.

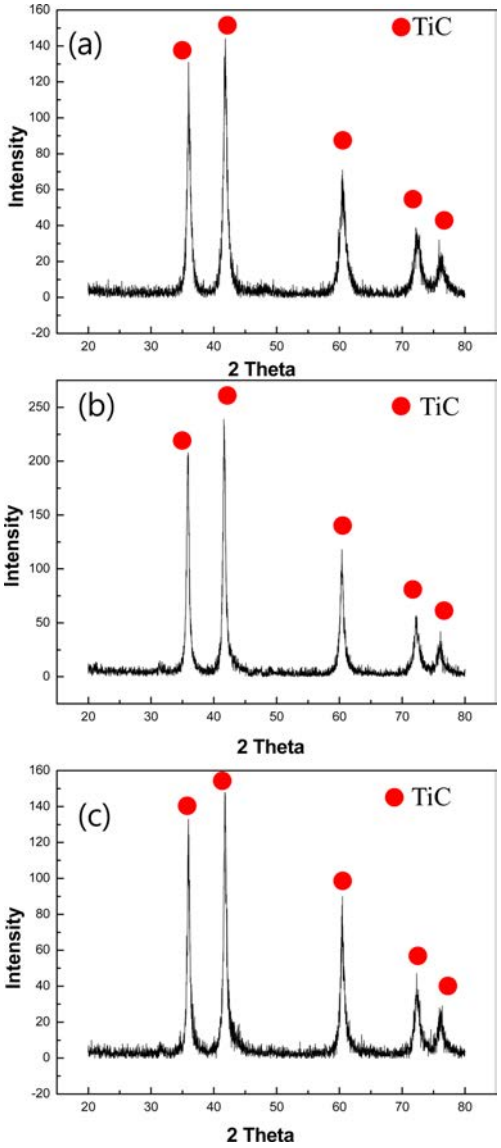

Fig. 3. XRD patterns of (a) TiC, (b) TiC-5 vol.%FeAl, and (c) TiC-10 vol.%FeAl powders milled for 10 h.

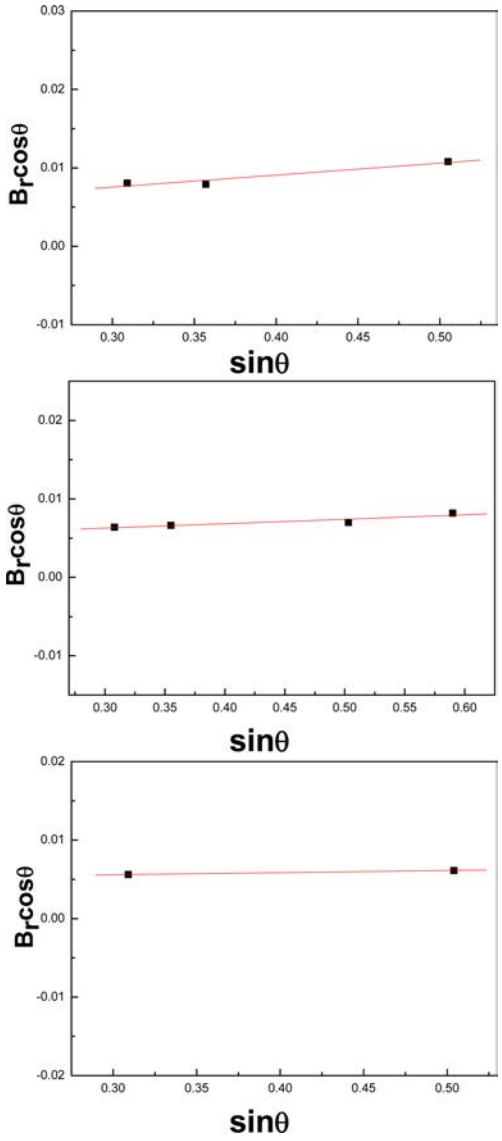

Fig. 4. Plot of Br ($B_{crystalline} + B_{strain}$) cosθ versus sinθ for TiC in (a) TiC, (b) TiC-5 vol.%FeAl, and (c) TiC-10 vol.%FeAl powders milled for 10 h.

Results and Discussion

FE-SEM images of TiC, TiC-5 vol.% FeAl, and TiC-10 vol.% FeAl powders milled for 10 h are shown in Fig. 2. The powders are very fine and have a round shape. Fig. 3 shows X-ray diffraction pattern of the TiC, TiC-5 vol.% FeAl, and TiC-10 vol.% FeAl powders after milling for 10 h. The broadening of TiC peaks due to crystallite refinement and strain is evident after milling for 10 h. The milling process is known to introduce impurities from the ball and/or container. However, in this study, peaks other than TiC were not identified. Fig. 4 shows plot of B_r ($B_{crystalline} + B_{strain}$) cosθ versus sinθ in Suryanarayana and Grant Norton's formula [20] to calculate particle size. The average grain sizes of the TiC in the TiC, TiC-5vol.% FeAl, and TiC-10 vol.% FeAl powders after milling for 10 h. calculated from the XRD data were about, 46, 30 and 28 nm, respectively.

The shrinkage displacement-time (temperature) curve provides an important information on the consolidation behavior. Fig. 5 shows the shrinkage record of TiC, TiC-5 vol.% FeAl, and TiC-10 vol.% FeAl compacts under the applied pressure of 80 MPa. In all cases, as induced current was applied, thermal expansion shows up to in the range 1000 and 1100 ºC according to FeAl content. And then shrinkage displacement abruptly increased above the temperature. The application of the induced current resulted in shrinkage due to consolidation. The temperature of rapid shrinkage initiation was seen to reduce by the addition of FeAl. It is considered that it is related to the melting of FeAl phase due to large Joule heat at contact of powders. Therefore, the main densification mechanism could be the rearrangement of carbide particles, enhancement of the diffusion, and

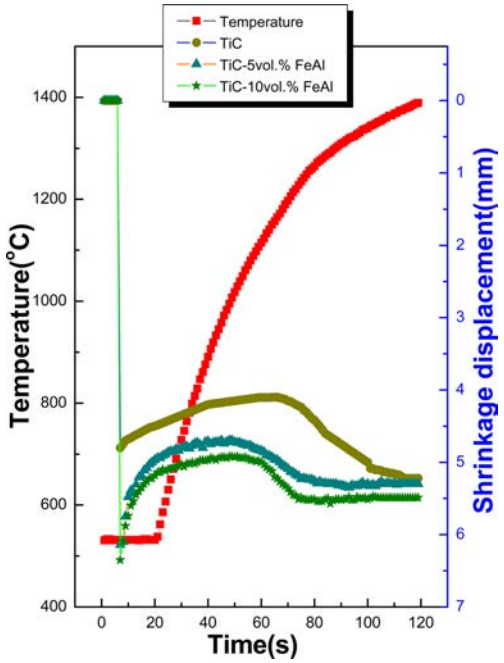

Fig. 5. Variations of temperature and shrinkage displacement with heating time during the sintering of TiC, TiC-5 vol.%FeAl, and TiC-10 vol.% FeAl hard materials by HFIHS.

viscous flow of the binder [21].

Fig. 6 shows the XRD patterns of TiC, TiC-5vol.% FeAl, and TiC-10 vol.% FeAl after sintering. In all cases, only TiC peaks are detected. The average grain sizes of the TiC calculated from the XRD data using Suryanarayana and Grant Norton's formula are about 90, 65, and 98 nm for the samples with TiC, TiC-5 vol.% FeAl, and TiC-10 vol.% FeAl. FE-SEM images of the samples after being sintered up to about 1400 ºC are shown in Fig. 7. It is apparent that the TiC grains consist of nanocrystallites suggesting the absence of grain growth during sintering. This retention of the fine grain structure can be attributed to the high heating rate and the relatively short exposure to the high temperature. Relative densities corresponding to TiC, TiC-5 vol.% FeAl, and TiC-10vol.% FeAl were approximately 98, 99, and 100%, respectively.

The role of the current in sintering and/or synthesis has been the focus of several attempts to provide an explanation for the observed sintering enhancement and the improved characteristics of the products. The role played by the current has been variously interpreted. The effect has been explained by fast heating due to Joule heating at contacts points, the presence of plasma in pores separating powder particles, and the intrinsic contribution of the current to mass transport [22-26].

Vickers hardness measurements were performed on polished sections of the TiC, TiC-5 vol.% FeAl, and TiC-10 vol.% FeAl samples using a 30 kg load and 15 s dwell time. Indentions with 30 kgf load produced median cracks around the indentation from which fracture toughness can be calculated. The lengths of these cracks

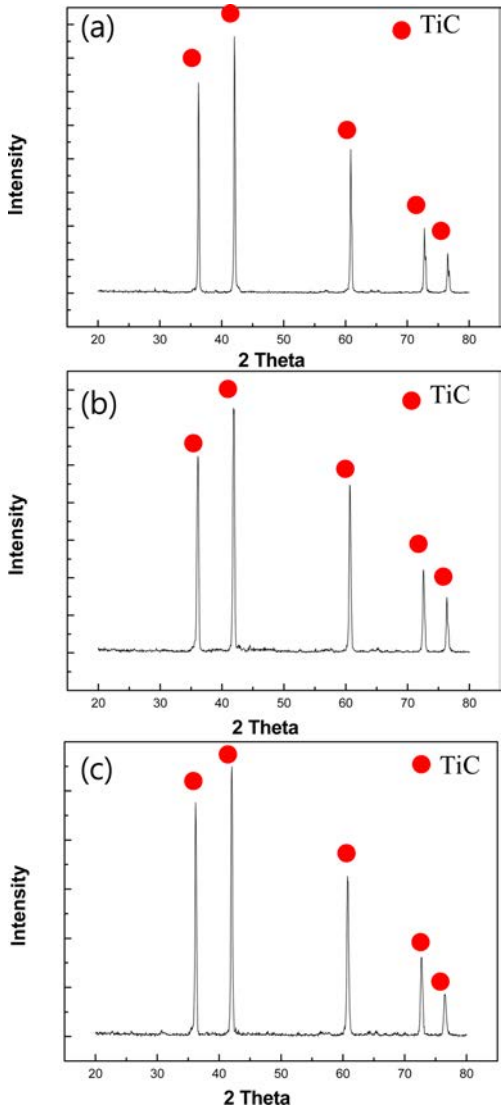

Fig. 6. XRD patterns of (a) TiC, (b) TiC-5 vol.%FeAl, and (c) TiC-10 vol.%FeAl hard materials produced by HFIHS.

permit estimation of the fracture toughness of the materials by means of the expression [27]:

$$KIC = 0.203(c / a)^{-3/2} \cdot Hv \cdot a^{1/2} \quad (2)$$

where c is the trace length of the crack measured from the center of the indentation, a is one half of the average length of the two indent diagonals, and H_v is the hardness.

The Vickers hardness and the fracture toughness values of the TiC, TiC-5 vol.% FeAl, and TiC-10 vol.% FeAl samples were 2518 kg/mm^2, 6.3 MPa · m$^{1/2}$, and 2430 kg/mm^2, 8.6 MPa · m$^{1/2}$ and 2290 kg/mm^2, 11.5 MPa · m$^{1/2}$, respectively. These values represent the average of five measurements. The fracture toughness of TiC-5 vol.% FeAl, and TiC-10 vol.% FeAl samples are higher than that of monolithic TiC without great decrease of hardness because the relative density of TiC increases with addition of

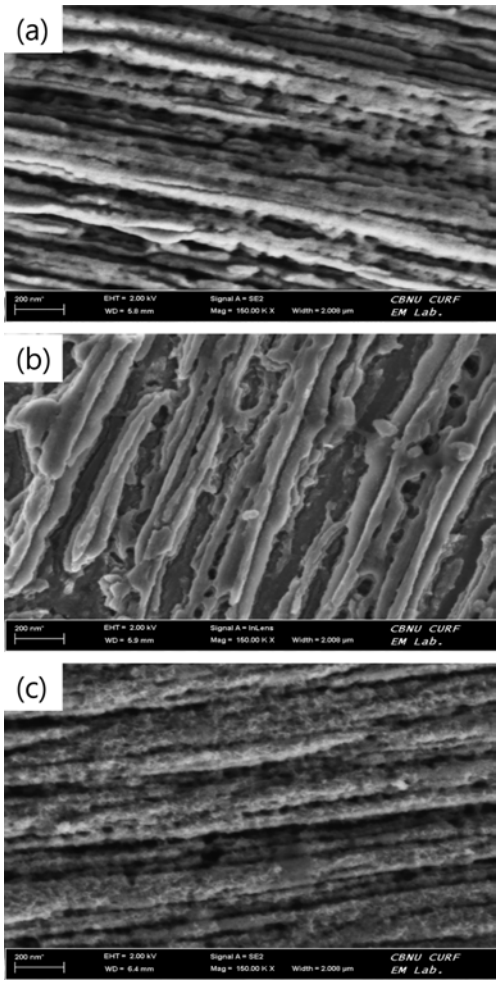

Fig. 7. FE-SEM images of (a) TiC, (b) TiC-5 vol.%FeAl, and (c) TiC-10 vol.%FeAl hard materials produced by HFIHS.

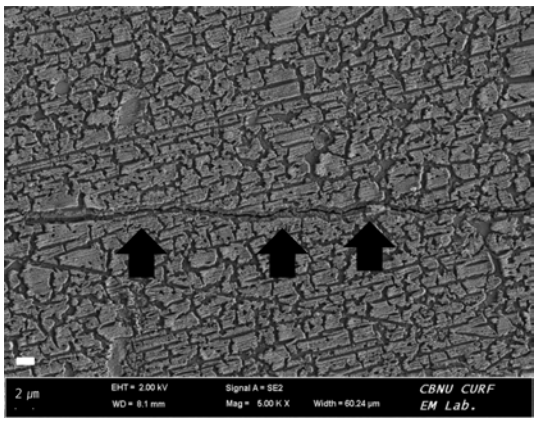

Fig. 8. Crack propagation in TiC- 10 Vol% FeAl hard materials produced by HFIHS.

FeAl. The sintering method in this study was proven to be very effective to consolidate TiC-FeAl cermets. The hardness of metal carbide greatly decreased by addition of Co or Ni [28]. The use of $TiAl_3$ binder instead of Co or Ni is very effective especially to maintain the high hardness of monolithic TiC without the expense of toughness reduction. In this regard, it would be worthwhile to consider FeAl as the possible replacement for Co or Ni especially for the applications requiring a high hardness.

Vickers hardness indentations in the TiC, TiC-5 vol.% FeAl, and TiC-10 vol.% FeAl samples show typically one to three additional cracks propagating radially from the indentation. Fig. 8 shows a crack propagated in a deflective manner (↑) in TiC-10 vol.% FeAl composite. The enhanced fracture toughness of TiC-10 vol.% FeAl composite is believed that TiC and FeAl in the composite may deter the propagation of cracks and TiC and FeAl have nanostructure phases.

Conclusions

Using high frequency induction heated sintering (HFIHS), the rapid consolidation of the TiC, TiC-5 vol.% FeAl, and TiC-10 vol.% FeAl was accomplished successfully. Nearly full-dense TiC-FeAl composites could be obtained within 2 min. The starting temperature of rapid densification and porosity of TiC were reduced remarkably by the addition of FeAl. The average grain sizes of the TiC are about 90, 65, and 98 nm for the samples with TiC, TiC-5 vol.% FeAl, and TiC-10 vol.% FeAl. The Vickers hardness and the fracture toughness values of the TiC, TiC-5vol.% FeAl, and TiC-10 vol.% FeAl samples were 2518 kg/mm^2, 6.3 MPa$\cdot$m$^{1/2}$, and 2430 kg/mm^2, 8.6 MPa$\cdot$m$^{1/2}$ and 2290 kg/mm^2, 11.5 MPa$\cdot$m$^{1/2}$, respectively. The addition of FeAl to TiC improved the fracture toughness of cemented TiC without great reduction of hardness. It would be worthwhile to consider FeAl as the possible replacement for Co or Ni especially for the applications requiring a high hardness.

Acknowledgments

This work was supported by a grant in aid awarded by the Basic Research Project of the Korea Institute of Geoscience and Mineral Resources (KIGAM), funded by the Ministry of Science, ICT and Future Planning (GP2015036) and following are results of a study on the “Leaders Industry-university Cooperation” Project, supported by the Ministry of Education, Science & Technology (MEST).

References

1. Imasato S, Tokumoto K, Kitada T, Sakaguchi S, Int J of Refract Met and Hard Mater 13 (1995) 305-12.
2. G Gille, J Bredthauer, B Gries, B Mende, Int J of Refract Met and Hard Mater 18 [2-3] (2000) 87-102.
3. P Goeuriot, F Thevenot, Ceramics International 13[2] (1987) 99-103.
4. Z.G. Zhang, F. Gesmundo, P.Y. Hou, Y. Niu, Corrosion Science 48 (2006) 741-765.
5. H Gleiter, Progress in Materials Science 33[4] (1989) 223-315.
6. GE Fougere, JR Weertman, RW Siegel, S Kim, Scripta

Metallurgica et Materialia 26 [2] (1992) 1879-1883.
7. M. Sherif El-Eskandarany, J. Alloys & Compounds 305 (2000) 225-38.
8. L Fu, LH Cao, YS Fan, Scripta Materialia 44 (2001) 1061-1068.
9. K Niihara, A Nikahira, Advanced structural Inorganic Composite, Elsevier Scientific Publishing Co., Trieste, Italy, 1990.
10. S Berger S, R Porat R, R Rosen, Progress in Materials, Progress in Materials 42 (1997) 311-320.
11. G.W. Lee, I.J. Shon, Korean J. Met. Mater. 51, (2013) 95-100.
12. I.J. Shon, G.W. Lee, J.M. Doh, J.K. Yoon, Electronic Materials Letters, 9, (2013) 219-225.
13. F. Charlot, E. Gaffet, B. Zeghmati, F. Bernard, J. C. Liepce, Mater. Sci. Eng. A262, (1999) 279-278.
14. W. Kim, C.Y. Suh, K.M. Roh, S.W. Cho, K.I Na, I.J. Shon, Journal of Alloys and Compounds 568 (2013) 73-77.
15. M.K. Beyer, H. Clausen-Schaumann, Chem. Rev. 105, (2005) 2921-2948.
16. In-Jin Shon, Ik-Hyun Oh, Jung-Han Ryu, Jun-Ho Jang, Hee-Jun Youn and Hyun-Kuk Park, Journal of Ceramic Processing Research. Vol. 14, No. 5 (2013) 641~647.
17. I.J. Shon, Korean J. Met. Mater. 52, (2014) 573-580.
18. Seung-Mi Kwak, Hyun-Kuk Park, and In-Jin Shon, Korean J. Met. Mater. 51, (2013) 341-348.
19. Na-Ra Park, Kwon-Il Na, Hanjung Kwon, Jae-Won Lim, and In-Jin Shon, Korean J. Met. Mater. 51, (2013) 753-759.
20. Suryanarayana C. and Grant Norton M., *X-ray Diffraction A Practical Approach*, Plenum Press, New York, 1998.
21. GS Upadhyaya, Materials & Design 22 [6] (2001) 483-489.
22. Z. Shen, M. Johnsson, Z. Zhao and M. Nygren, J. Am. Ceram. Soc. 85 (2002) 1921-1927.
23. J. E. Garay, U. Anselmi-Tamburini, Z. A. Munir, S. C. Glade and P. Asoka- Kumar, Appl. Phys. Lett. 85 (2004) 573-575.
24. J. R. Friedman, J. E. Garay. U. Anselmi-Tamburini and Z. A. Munir, Intermetallics. 12 (2004) 589-597.
25. J. E. Garay, J. E. Garay. U. Anselmi-Tamburini and Z. A. Munir, Acta Mater., 51 (2003) 4487-4495.
26. Rishi Raj, Marco Cologna, and John S. C. Francis, J. Am. Ceram. Soc., 94 [7] (2011) 1941-1965.
27. K. Niihara, R. Morena, and D. P. H. Hasselman, J. Mater. Sci. Lett. 1 (1982) 12-16.
28. In-Jin Shon, In-Kyoon Jeong, In-Yong Ko, Jung-Mann doh, Kee-Do Woo, Ceramics International 35 (2009) 339-344.